

# Studying Attractor Symmetries by Means of Cross Correlation Sums

Peter Schneider and Peter Grassberger

Physics Department, University of Wuppertal, D-42097 Wuppertal, Germany

November 14, 2018

## Abstract

We use the cross correlation sum introduced recently by H. Kantz to study symmetry properties of chaotic attractors. In particular, we apply it to a system of six coupled nonlinear oscillators which was shown by Kroon *et al.* to have attractors with several different symmetries, and compare our results with those obtained by “detectives” in the sense of Golubitsky *et al.*.

Keywords: deterministic chaos, symmetric attractors, symmetry detection, cross correlation sums

# 1 Introduction

Spontaneous symmetry breaking is one of the most interesting problems in statistical physics. While in the past most work has been done on equilibrium systems, it has become clear only recently that very interesting similar phenomena occur also in non-equilibrium systems. Indeed, the variety of phenomena observed there is even larger than in equilibrium models, even if we restrict ourselves to purely deterministic (but in general chaotic) systems as we shall do in the present work. Spontaneous symmetry breaking, in particular, can be of two fundamentally different kinds.

Assume that the equation of motion

$$\frac{d\mathbf{x}(t)}{dt} = \mathbf{F}(\mathbf{x}(t)) \quad (1)$$

(with  $\mathbf{x}(t)$  in some manifold  $\mathcal{M}$ ) is *equivariant* (or “covariant” in the physics literature) under some symmetry group  $G$  acting on  $\mathcal{M}$ , i.e.

$$g\mathbf{F}(\mathbf{x}) = \mathbf{F}(g\mathbf{x}) \quad (2)$$

for each element  $g \in G$ . We assume that  $\mathbf{F}$  has at least one chaotic or quasiperiodic attractor.

In such a case, orbits  $\mathbf{x}(t)$  can have the following symmetry properties:

- (1) They are symmetric under each element  $g \in G$ , i.e.  $g\mathbf{x}(t) = \mathbf{x}(t)$ , for each  $g \in G$ .
- (2) Individual orbits are symmetric only with respect to some subgroup  $\Sigma \subset G$ , but the attractor and the invariant measure are still symmetric under  $G$ . Notice that  $\Sigma$  can be trivial (having just the identity as unique element), in which case the *instantaneous* symmetry is maximally broken, while the symmetry of the attractor is still unbroken. Such a case occurs most naturally when the system is composed of two identical subunits and  $G$  is just the permutation group of two elements interchanging them. The transition from item 2 to item 1 manifests itself then in synchronization of the two subunits [1, 2, 3]. Thus (de-)synchronization is just the simplest version of a sort of spontaneous symmetry breaking, and it was stressed in [4] that the breaking of other symmetries should follow essentially the same lines.
- (3) Also the attractor is no longer symmetric under the full group  $G$ , but only under some subgroup  $\Sigma \subset G$  (the “symmetry group” of the attractor). In this case one has of course coexistence of several attractors related to each other by symmetry transformations  $g \in G/\Sigma$ . Transitions between item 1 and item 3 are possible [5] but less common than transitions either between 1 and 2 or between 2 and 3. The latter have been studied intensively in [6, 7, 8]. In the most frequent scenario, the different attractors in the symmetry broken phase are disjoint, and symmetry is restored when these attractors touch in one or several points.

In the present paper we shall only deal with item 3, and with transitions between 2 and 3. We shall not deal with item 1 or with transitions between 1 and 2. More precisely, we shall study the following problem [9, 10, 11]: we are given a time series generated by  $\mathbf{F}$ , and we want to estimate the maximal subgroup  $\Sigma \in G$  under which the natural invariant measure (*BRS-measure* [12]) is invariant,

$$\mu(B) = \mu(h^{-1}B), \quad h \in \Sigma. \quad (3)$$

Here,  $B$  is any measurable set intersecting the attractor, and we assume that the initial conditions for the time series are  $\mu$ -random. Since this is a statistical decision problem, we cannot expect an unambiguous answer. In a proper treatment we should work out the detailed statistics of any used observable, and obtain the corresponding significance criteria. Following [9, 10, 11] and a venerable tradition established in physics, we shall not do so here but hope that the results will be so clear cut that such formal significance criteria will not be necessary.

In order to find the symmetry of a measure  $\mu$  from a set of  $N$  points  $\mathbf{x}_k$ ,  $k = 1 \dots N$  drawn randomly from this measure, there are several possible strategies.

(a) Visual inspection. For low dimensions, this is of course the method of choice. At higher dimensions, we can still visualize by making projections or cross sections. But usually, these will be less informative and more cumbersome.

(b) We can partition phase space in some way such that each  $g \in G$  acts as a permutation  $P_g$  on the elements  $\mathcal{U}_i$  of the partition,

$$g \mathcal{U}_i = \mathcal{U}_j, \quad j = P_g i. \quad (4)$$

If the measure is symmetric, then we have

$$\mu(\mathcal{U}_i) = \mu(\mathcal{U}_{P_g i}). \quad (5)$$

Therefore, if the time series points are iid (identically and independently distributed), then

$$n_i \approx n_{P_g i} \pm O(\sqrt{n_i}), \quad (6)$$

where  $n_i$  is the number of points in  $\mathcal{U}_i$ . In simple cases this can be very efficient, but it becomes very unwieldy in high dimensions and if  $G$ -invariant partitions are tricky to construct.

(c) We can consider averages over functions which themselves are not invariant under  $G$ . Assume that  $\phi(\mathbf{x})$  is such a function. Then

$$\langle \phi \rangle \equiv N^{-1} \sum_{k=1}^N \phi(\mathbf{x}_k) \quad (7)$$

will in general be different from

$$\langle g\phi \rangle = N^{-1} \sum_{k=1}^N \phi(g^{-1}\mathbf{x}_k) \quad (8)$$

unless  $\mu$  is invariant under  $g$ . Functions  $\phi$  for which  $\langle \phi \rangle = \langle g\phi \rangle$  *only* if  $\mu$  is invariant are called *detectives* in [9, 10, 11] (see these references for a more precise definition), and the numerical study of symmetry properties in these papers is based mainly on this method and on visual inspection of projections.

(d) In the present paper, we shall use yet another method based on an idea by H. Kantz [13]. In that work, the author was concerned with the more general problem of verifying numerically whether two measures are identical, making use of two random samples of points drawn from these measures. It uses the *cross correlation sum*, a generalization of the correlation sum used e.g. in estimates of the correlation dimension.

Assume that the two sets of points are  $X = \{\mathbf{x}_k, k = 1 \dots N\}$  and  $Y = \{\mathbf{y}_k, k = 1 \dots N\}$ . They are randomly drawn from the same space, but according to two different measures  $\mu$  and  $\nu$ . The correlation sum for the set  $X$  is defined as

$$C_{XX}(\epsilon) = \frac{1}{N(N-1)} \sum_{\mathbf{x}, \mathbf{y} \in X; \mathbf{x} \neq \mathbf{y}} \Theta(\epsilon - |\mathbf{x} - \mathbf{y}|) \quad (9)$$

where  $\Theta$  is the Heavyside step function. Thus  $C_{XX}$  measures the fraction of pairs having a distance  $< \epsilon$ . The cross correlation sum is defined similarly by

$$C_{XY}(\epsilon) = \frac{1}{N^2} \sum_{\mathbf{x} \in X} \sum_{\mathbf{y} \in Y} \Theta(\epsilon - |\mathbf{x} - \mathbf{y}|) . \quad (10)$$

Obviously,  $C_{XY} \approx C_{XX}$  up to statistical fluctuations if  $X$  and  $Y$  are distributed according to the same measure. Otherwise, we expect an inequality. More precisely, let us define the cross correlation *integral* by

$$C_{\mu\nu}(\epsilon) = \int d\mu(\mathbf{x}) \int d\nu(\mathbf{y}) \Theta(\epsilon - |\mathbf{x} - \mathbf{y}|) . \quad (11)$$

Almost surely,  $C_{XY}(\epsilon) \rightarrow C_{\mu\nu}(\epsilon)$  for  $N \rightarrow \infty$ , and  $C_{XY}(\epsilon)$  is an unbiased estimator for  $C_{\mu\nu}(\epsilon)$  in the sense that  $C_{\mu\nu}(\epsilon) = \langle C_{XY}(\epsilon) \rangle$  where the brackets denote the average over different random samples  $X$  and  $Y$ . For sufficiently small  $\epsilon$  and for absolutely continuous measures  $\mu$  and  $\nu$  one can then show [13]

$$C_{\mu\nu}^2(\epsilon) \leq C_{\mu\mu}(\epsilon) C_{\nu\nu}(\epsilon) . \quad (12)$$

Unfortunately, the same is not necessarily true for  $C_{XY}(\epsilon)$  with finite  $N$  [13], due to the omission of “diagonal” terms in the double sum in eq.(9). This omission is necessary since otherwise  $C_{XX}(\epsilon)$  would be a biased estimator for  $C_{\mu\mu}(\epsilon)$ . Nevertheless, the analogon of eq.(12) for finite  $N$  will be violated only in exceptional cases due to statistical fluctuations, and only if  $\mu \approx \nu$ .

Also, eq.(12) cannot be shown for all  $\epsilon$  and for arbitrary measures. This follows from Bochner’s theorem and the fact that the Fourier transform of  $\Theta(\epsilon - |\mathbf{x}|)$  is not positive definite. To avoid this problem, we could e.g. replace  $\Theta$  by a Gaussian,

so that  $C_{\mu\nu}(\epsilon) = \int d\mu(\mathbf{x}) \int d\nu(\mathbf{y}) e^{-(\mathbf{x}-\mathbf{y})^2/\epsilon}$  and similarly for the discrete cross correlation sums. We did not do this since this would make the numerics less efficient, and since we did not encounter any practical problems when using eq.(10) in the applications described in sec.3.

Thus we use as a similarity measure the cross correlation ratio

$$r(\epsilon) = \frac{C_{XY}(\epsilon)}{\sqrt{C_{XX}(\epsilon)C_{YY}(\epsilon)}} . \quad (13)$$

For very large  $\epsilon$  it is equal to 1 since  $C_{XY}(\epsilon) = C_{XX}(\epsilon) = C_{YY}(\epsilon) = 1$  for sufficiently large  $\epsilon$  (we assume that the measures have compact support). On the other extreme,  $r(\epsilon) \rightarrow 0$  for  $\epsilon \rightarrow 0$  if the measures  $\mu$  and  $\nu$  have disjoint supports. The latter is typically [6] but not always [5] true if  $\mu$  is a (time) invariant measure which is not invariant under some  $g \in G$ , and  $\nu$  is the  $g$ -image of  $\mu$ . For intermediate values of  $\epsilon$  we expect a monotonic increase, though we cannot exclude a more complex behavior. We can define a characteristic distance  $\epsilon_c$  between the sets  $X$  and  $Y$  by demanding for instance  $r(\epsilon_c) = 1/2$ .

In the present application,  $X$  is a time series and  $Y$  is just the image of  $X$  under a group action  $g$ ,

$$Y = gX \equiv \{g\mathbf{x} \mid \mathbf{x} \in X\} . \quad (14)$$

Furthermore, we assume that the norm  $|\cdot|$  is invariant under  $g$  (in the following, we use Euclidean norm). Thus  $C_{YY} = C_{XX}$ , and the cross correlation ratio for element  $g$  is equal to

$$r_g(\epsilon) = \frac{C_{X,gX}(\epsilon)}{C_{XX}(\epsilon)} . \quad (15)$$

A problem arises from the fact that points in a time series are correlated and do thus not form a sample of iid points. This has mainly two more or less disjoint effects. The first is that it might take rather long until an orbit visits all parts of the attractor. This is particularly important in the vicinity of a bifurcation, and when there is intermittency or transients with very long characteristic times  $\tau$ . In such cases the only remedy is to take time sequences which span a total time  $T \gg \tau$ . To avoid huge data sets, one should then decimate the data. We thus take

$$\mathbf{x}_n = \mathbf{x}(nm \, dt) , \quad n = 1, \dots, N \quad (16)$$

where  $dt$  is the integration step and  $m$  is a sufficiently large integer. Independent from this, data on short scales might be correlated on time scales  $t < t_{corr}$  with  $t_{corr} > m \, dt$ . In this case, even the decimated data are correlated. As pointed out by Theiler [14], it is then necessary to omit pairs in eqs.(9,10) whose indices differ by less than  $n_0 = t_{corr}/m \, dt$ . Thus our final formula for  $r_g(\epsilon)$  is

$$r_g(\epsilon) = \frac{\sum \sum_{i,k=1}^N \Theta(\epsilon - |\mathbf{x}_i - g\mathbf{x}_k|) \Theta_{|i-k| \geq n_0}}{\sum \sum_{i,k=1}^N \Theta(\epsilon - |\mathbf{x}_i - \mathbf{x}_k|) \Theta_{|i-k| \geq n_0}} . \quad (17)$$

Finally let us discuss some immediate consequences following from the facts that  $C_{XY}$  is symmetric under the exchange  $X \leftrightarrow Y$ , that  $G$  is a group, and that the norm is invariant under  $G$ . The first is that  $C_{X,gX} = C_{gX,X} = C_{X,g^{-1}X}$  for all  $g \in G$ , and hence

$$r_g(\epsilon) = r_{g^{-1}}(\epsilon), \quad g \in G. \quad (18)$$

Next assume that  $h$  is in the symmetry group  $\Sigma$  of the attractor. Then  $hX \approx X$  and thus  $C_{X,gX} \approx C_{X,ghX} \approx C_{X,hgX}$  with errors vanishing for  $N \rightarrow \infty$ . This implies that  $r_g$  takes the same value in the entire left and right cosets of  $\Sigma$ ,

$$r_g(\epsilon) = r_{gh}(\epsilon) = r_{hg}(\epsilon), \quad h \in \Sigma, \quad g \in G, \quad (19)$$

up to statistical fluctuations.

## 2 Numerical Example

Since we want to test our method against the method of detectives [9, 10, 11], we use exactly the same model as in [11]. It models the gait of a hexapodal animal, and is described in detail in [15]. It involves six identical nonlinear oscillators, coupled in a ring-like fashion. More precisely, the equations of motion are (note the misprint in the second line in [11])

$$\begin{aligned} \frac{dx_p}{dt} &= -4x_p + y_p + (x_p^2 + y_p^2)(Px_p - Qy_p) - \\ &\quad - \lambda(4(x_{p-1} + x_{p+1}) - 2(y_{p-1} + y_{p+1})) \\ \frac{dy_p}{dt} &= -x_p - 4y_p + (x_p^2 + y_p^2)(Py_p + Qx_p) - \\ &\quad - \lambda(2(x_{p-1} + x_{p+1}) + 4(y_{p-1} + y_{p+1})), \quad p = 0, 1, \dots, 5 \pmod{6}. \end{aligned} \quad (20)$$

The system is equivariant under cyclic or anticyclic permutations of the indices of the oscillators. This would give the dihedral group  $\mathbf{D}_6$  as equivariance group. It consists of 12 permutations and is a subgroup of  $\mathbf{S}_{12}$ . Its generators are

$$\kappa = \begin{pmatrix} 0 & 1 & 2 & 3 & 4 & 5 \\ 0 & 5 & 4 & 3 & 2 & 1 \end{pmatrix} \quad (21)$$

$$\zeta = \begin{pmatrix} 0 & 1 & 2 & 3 & 4 & 5 \\ 1 & 2 & 3 & 4 & 5 & 0 \end{pmatrix}. \quad (22)$$

But in addition, the above system has a  $\mathbf{Z}_2$  symmetry  $(x_p, y_p) \rightarrow (-x_p, -y_p)$  which was missed in [11]. Thus the full equivariance group is

$$G = \mathbf{D}_6 \times \mathbf{Z}_2 \quad (23)$$

Attractors can have as symmetry groups any subgroup of  $G$ . Disregarding the factor  $\mathbf{Z}_2$  for the moment, the subgroups of  $\mathbf{D}_6$  are (up to conjugacies)  $\mathbf{1}$ ,  $\mathbf{Z}_2 = \{1, \zeta^3\}$ ,  $\mathbf{Z}_3$ ,  $\mathbf{Z}_6$ ,  $\mathbf{D}_1 = \{1, \kappa\}$ ,  $\tilde{\mathbf{D}}_1 = \{1, \kappa\zeta\}$ ,  $\mathbf{D}_2$ ,  $\mathbf{D}_3$ ,  $\tilde{\mathbf{D}}_3$  and  $\mathbf{D}_6$ .

In [11], the attractor was projected for visual inspection onto a two dimensional subspace by means of the variables

$$u = x_1 - x_2 + x_4 - x_5 \quad (24)$$

and

$$v = \frac{1}{\sqrt{3}}(x_1 + x_2 - 2x_3 + x_4 + x_5 - 2x_0) . \quad (25)$$

In the  $(u, v)$  plane, the action of  $\zeta$  is a clockwise (negative) rotation by an angle  $2\pi/3$ , while  $\kappa$  corresponds to a reflection on the axis  $u = 0$ . Notice that this is not a faithful representation of  $\mathbf{D}_6$  since  $\zeta^3$  is represented by the unity  $(u, v) \rightarrow (u, v)$ . The figures shown in [11] suggest that all attractors are symmetric under the additional  $\mathbf{Z}_2$  symmetry. This was also verified by ourselves in all cases, whence we shall disregard this  $\mathbf{Z}_2$  in the following and consider only symmetry under the elements of  $\mathbf{D}_6$ .

As distance measure in the correlation sums we used  $r = [\sum_p (x_p - x'_p)^2 + \sum_p (y_p - y'_p)^2]^{1/2}$ .

Since our goal was to compare the correlation sum method to the method of detectives, we followed [11] in keeping the parameters  $P$  and  $\lambda$  fixed at  $P = -5$  and  $\lambda = 1.2$ . The parameter  $Q$  was used as control parameter and was varied in the range  $25.0 \leq Q \leq 27.2$  studied also in [11].

We integrated eq.(21) with a fourth order Runge-Kutta algorithm with time step  $dt = 0.01$ . Again this was done in order to compare with [11]. This time step might be too large for some of the  $Q$ -values considered, whence some of the observed structures might be artefacts of the time discretization. But this is not much of a concern: the time discretized system is as good a nonlinear dynamical system as the ODE, and studying its symmetries should be neither more easy nor more difficult.

An important point where we departed from [11] was the global time scales. We found that several of the attractors described in [11] represented actually transients (e.g. for  $Q = 26.9$ , the final attractor is as shown in fig.3 below, and not as described in [11]). Thus we discarded in all cases a transient of length  $t \geq 10000$ . In addition, we have the problem of long residence times on parts of the entire attractor discussed already in [11]. This gives rise to fake attractor asymmetries if the length of the time series is less than these residence times. To avoid this, we took only every 550th point<sup>1</sup>, i.e.  $m dt \approx 5$  (see eq.(16)). Finally, we used a Theiler cutoff  $n_0 = 100$ .

Another point where we departed from [11] was the number of points used. While the analysis of [11] was based on 10,000 - 50,000 points for each value of  $Q$ , we used only 5,000 points. This was done not only for minimizing the computational effort

---

<sup>1</sup>For quasiperiodic attractors we found that large spurious correlations with very slow temporal decay could arise from near commensurability between the sampling frequency and some internal frequency of the attractor. To avoid this, we actually used an irregular sampling where we selected  $m$  randomly between 100 and 1000, such that  $\langle m \rangle = 550$ . Without this trick, we would have obtained  $r_g(\epsilon) \gg 1$  in several cases.

(which is higher for our method), but also to demonstrate that our method is very efficient already for small data samples.

A last remark: as one should expect in general, we found in some cases that the system possessed several attractors which are not related by symmetry. For instance, depending on the initial conditions we found for  $Q = 25.7$  either the attractor shown in [11] or another one which closely resembles the one found in [11] at  $Q = 25.6$ .

### 3 Results

In figures 1 to 4 we show four typical attractors together with the corresponding (cross-) correlation sums. For visualizing the attractors, we use the projection given by eqs.(24),(25). In each correlation sum plot, the number of pairs closer than  $\epsilon$  are plotted against  $\epsilon$  for each of the ten group elements  $g = 1, \zeta, \zeta^2, \zeta^3, \kappa, \kappa\zeta, \kappa\zeta^2, \kappa\zeta^3, \kappa\zeta^4$  and  $\kappa\zeta^5$ . Results for the remaining elements  $\zeta^4$  and  $\zeta^5$  are not shown since they

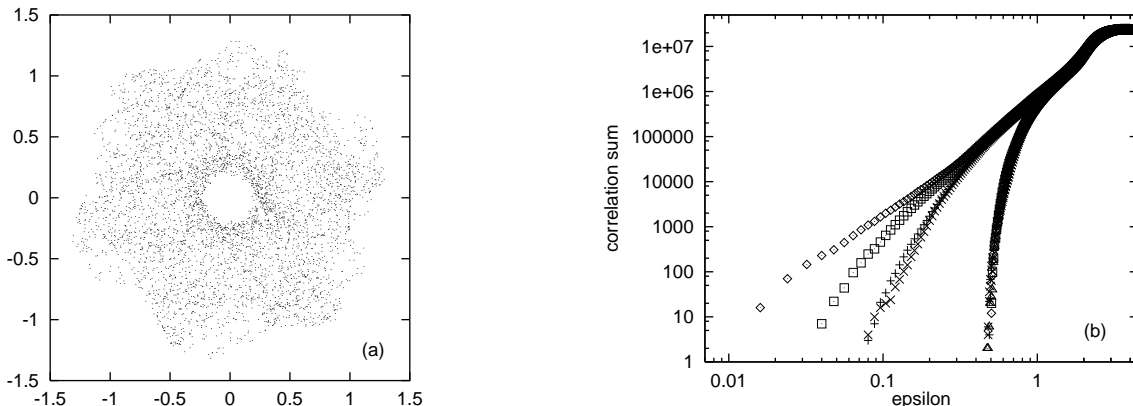


Figure 1: Panel (a): attractor for  $Q = 25.04$  projected onto the  $(u, v)$ -plane by means of eqs.(24,25). Panel (b): log-log plot of the cross and auto correlation sums (without normalization factors  $N^{-2}$ ) for  $Q = 25.04$ . The different symbols have the following meaning:  $\diamond$ :  $g = 1$  or  $\kappa\zeta^2$ ;  $+$ :  $g = \zeta$  or  $\kappa\zeta^3$ ;  $\square$ :  $g = \zeta^2$  or  $\kappa\zeta^4$ ;  $\times$ :  $g = \zeta^3$  or  $\kappa\zeta^5$ ;  $\triangle$ :  $g = \kappa$ ;  $*$ :  $g = \kappa\zeta$ .

coincide due to eq.(18) identically with those for  $\zeta^2$  and  $\zeta$ , respectively. Also, as we said already in the last section, we do not show the cross correlations for the inversion  $(\mathbf{x}, \mathbf{y}) \rightarrow (-\mathbf{x}, -\mathbf{y})$  since all attractors were found to be symmetric under it. We show the numbers of pairs instead of the correlation sums with conventional normalization as in eq.(9), since the square roots of these numbers give rough estimates of statistical errors for small values of  $\epsilon$  where these errors are most important (for rigorous error estimates of autocorrelation sums, see [16, 17]).

If an attractor is symmetric with respect to a group element  $g$ , we expect the corresponding  $C_{X,gX}$  to coincide with  $C_{X,X}$ . Within the expected statistical errors, the symmetries found in this way were also verified visually in the projections, except for  $g = \zeta^3$  which is mapped by the projection (24),(25) onto the unit element. Thus



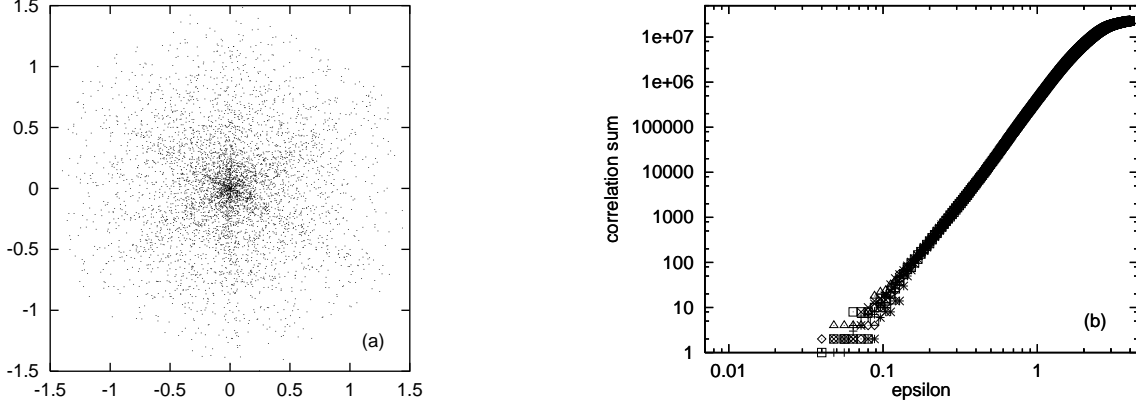


Figure 2: Same as fig.1, but for  $Q = 27.2$ .

invariance under  $\zeta^3$  cannot be read off from figures 1a to 4a, and can be seen only from the corresponding correlation sum plots.

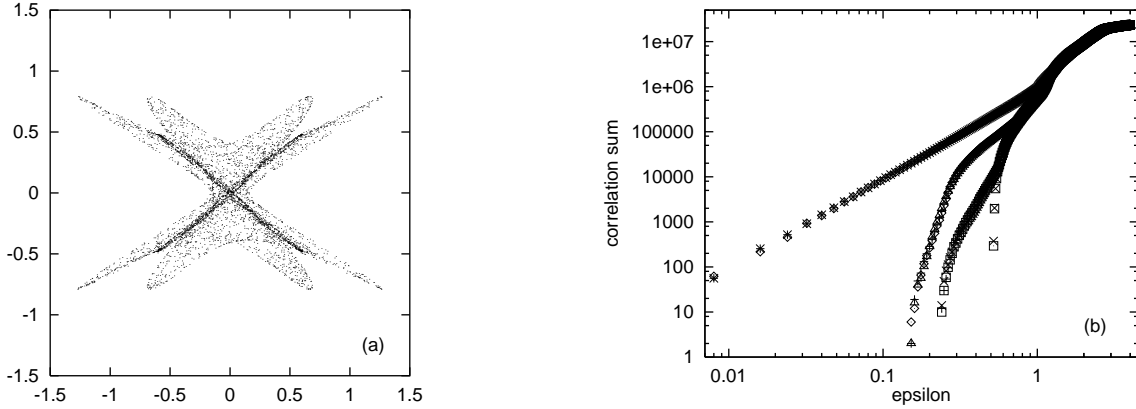


Figure 3: Same as fig.1, but for  $Q = 26.9$ .

In fig.1, the projection suggests a symmetry under the inversion  $(u, v) \rightarrow (-u, -v)$ , and maybe even under a rotation by  $60^\circ$ . We might be tempted to interpret this as invariance of the original attractor under  $\mathbf{Z}_2$  or  $\mathbf{Z}_6$ . From the correlation sums we see that this is not correct. Apart from the inversion  $(\mathbf{x}, \mathbf{y}) \rightarrow (-\mathbf{x}, -\mathbf{y})$ , the attractor has no symmetry at all, since none of the cross correlations agrees with the auto correlation sum (we notice that the invariance under  $(u, v) \rightarrow (-u, -v)$  seen in all figures in [11] is due to this inversion, and is not due to the particular projection used).

The other extreme of a completely symmetric attractor is shown in fig.2. We see that all cross correlation sums coincide.

An example of  $\tilde{\mathbf{D}}_1$  invariance is shown in fig.3. In the correlation sum plot we see four different curves. The one on top contains  $C_{X,X}$  and  $C_{X,\kappa\zeta X}$ . The other curves contain  $C_{X,\zeta X}$ ,  $C_{X,\kappa X}$ ,  $C_{X,\kappa\zeta^2 X}$  (second from top),  $C_{X,\zeta^2 X}$ ,  $C_{X,\kappa\zeta^3 X}$ ,  $C_{X,\kappa\zeta^5 X}$  (third from top), and  $C_{X,\zeta^3 X}$ ,  $C_{X,\kappa\zeta^4 X}$  (bottom/rightmost curve). This degeneracy

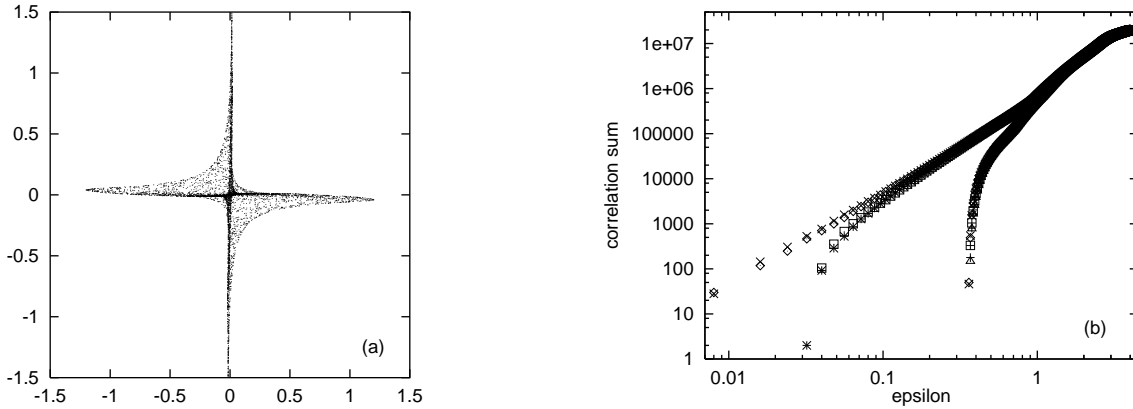


Figure 4: Same as fig.1, but for  $Q = 26.1$ .

of curves follows immediately from eq.(19) and the detailed group structure of  $\mathbf{D}_6$ .

Finally, we show in fig.4 a case with  $\mathbf{Z}_2$  symmetry. We seem to see there three curves, but the rightmost one indeed consists of a triplet of lines which can only be resolved at higher resolution. Thus we have five curves altogether, each corresponding to two cross correlation sums. This is exactly as expected from eq.(19). The near degeneracy of the rightmost three lines is explained by the very weak breaking of  $\mathbf{D}_2$  symmetry which is also seen in the fact that the two top curves are not very different except for very small  $\epsilon$ .

In all examples (including many more which are not shown here), the symmetry suggested by the correlation sums is compatible with that seen by looking at the  $(u, v)$ -projection of the attractor.

For a systematic investigation we have repeated this analysis for all values of  $Q \in [25.0, 27.2]$  in steps of  $\Delta Q = 0.01$  (221 values altogether). We repeated this three times with different types of initial conditions, in order to test for multiple attractors. In the first set of runs, we used the same initial values for all  $Q$ . In the second, different random initial conditions were used for each  $Q$ . Finally, in the third set of runs we used the last configuration from the simulation with  $Q$  as initial condition for simulating at  $Q + \Delta Q$ . In some cases (such as  $Q = 2.57$ , e.g.) this gave clear indications of multiple attractors which are not simply rotated images of each other.

Plots of cross correlation sum ratios against  $Q$  are shown in figures 5-10. These plots show results from the third type of initial conditions<sup>2</sup>, but the plots obtained with the other two types of initial conditions were very similar. Each figure corresponds to one group element. In each figure, three curves are shown. They represent  $r_g(\epsilon)$  at those three values of  $\epsilon$  where the unnormalized autocorrelation sum was equal to 1000, 3000 and 10,000, respectively. In this way we guaranteed that the statistical errors were roughly independent of  $Q$ , although the size of the attractor

<sup>2</sup>For simplifying the figures, each attractor was first brought by a conjugacy into a standard orientation such that the maximal  $r_g$  for reflexions  $g = \kappa\zeta^n$ ,  $n = 0 \dots 5$ , was obtained at either  $g = \kappa$  or  $g = \kappa\zeta$ .

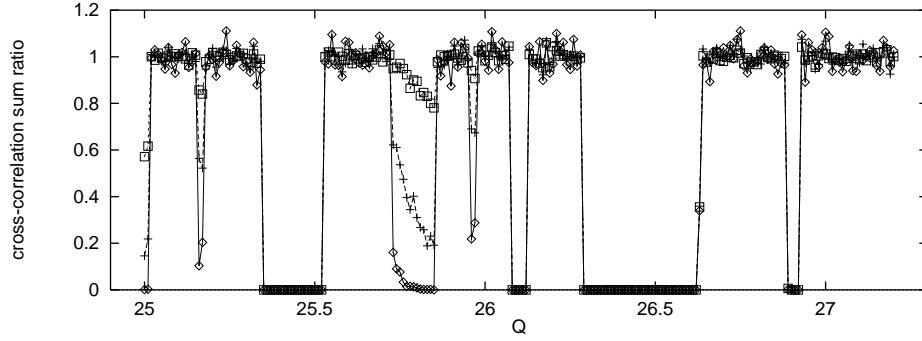


Figure 5: Cross correlation coefficients  $r_g(\epsilon)$  for  $g = \zeta$ , plotted against  $Q$ . Three data sets are superimposed, for distances  $\epsilon$  at which 1000, 3000 and 10,000  $\epsilon$ -close pairs were found. The corresponding symbols are  $\diamond$  (1000),  $+$  (3000), and  $\square$  (10,000).

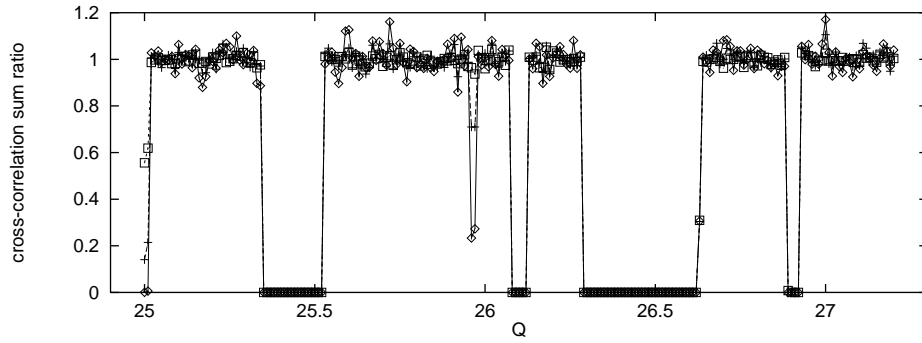


Figure 6: Same as fig.5, but for  $g = \zeta^2$ .

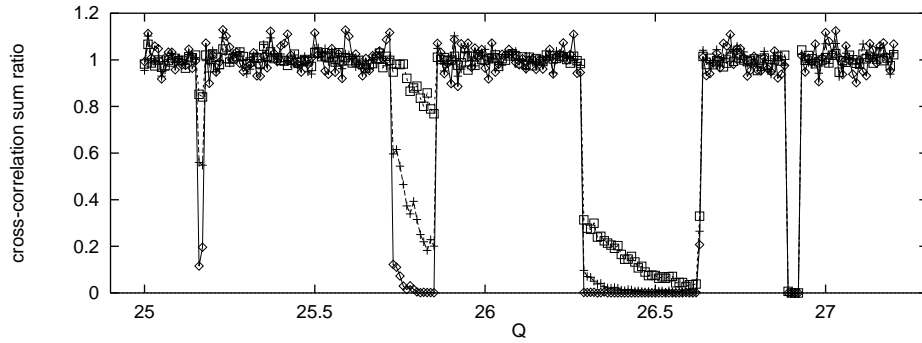


Figure 7: Same as fig.5, but for  $g = \zeta^3$ .

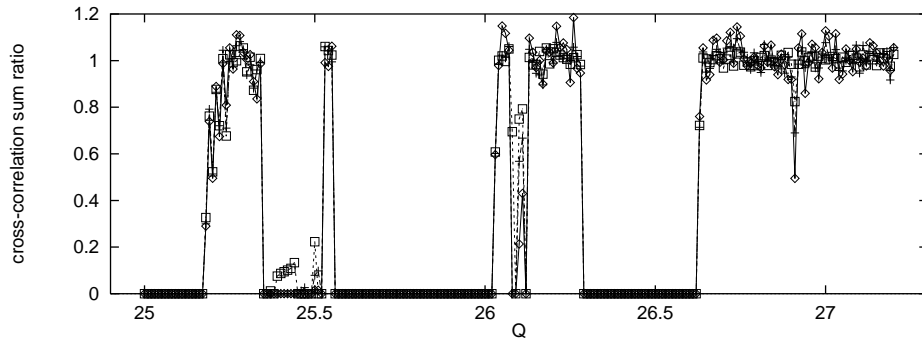


Figure 8: Same as fig.5, but for  $g = \kappa$ .

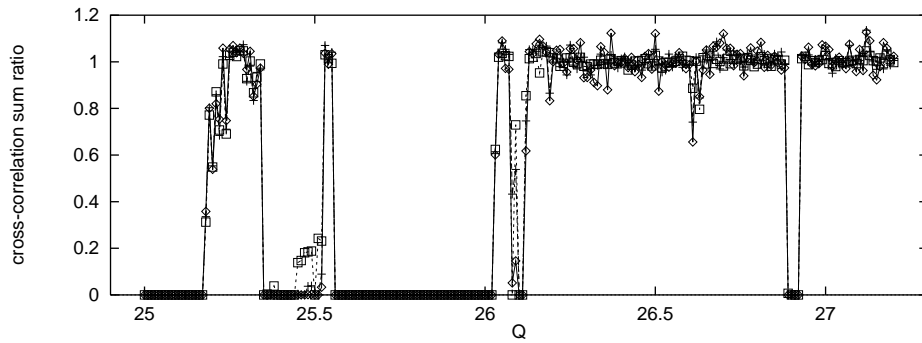


Figure 9: Same as fig.5, but for  $g = \kappa\zeta$ .

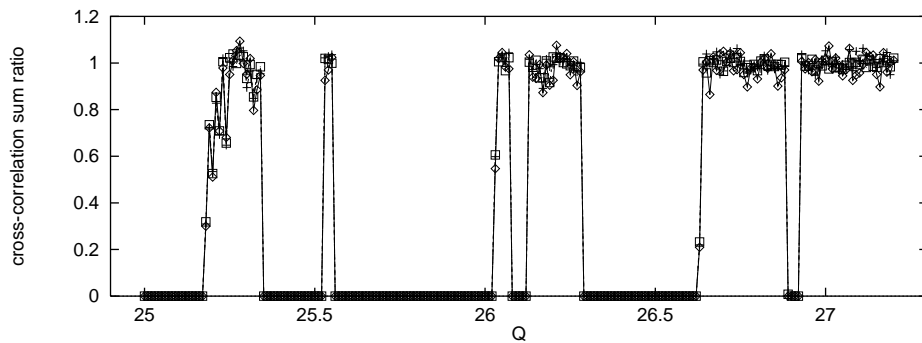


Figure 10: Same as fig.5, but for  $g = \kappa\zeta^2$ .

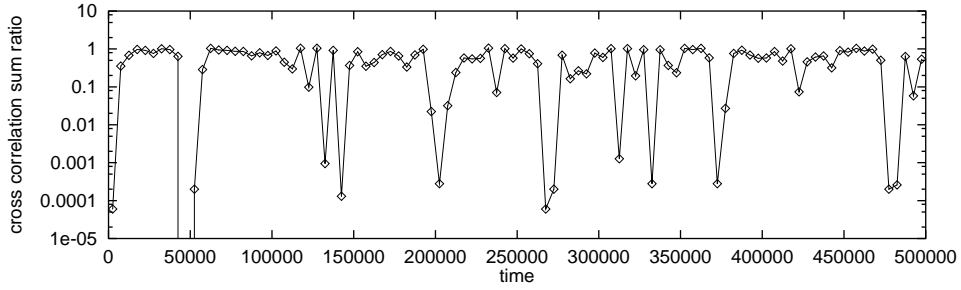


Figure 11: Cross correlation coefficient for  $g = \kappa$ ,  $Q = 25.22$  and  $\epsilon = 0.36$  plotted against time. For this, a very long time series was cut into pieces each containing 5000 points, and correlation coefficients were computed for each piece independently. On the horizontal axis is plotted physical time. In contrast to the previous plots, the average sampling frequency is  $\approx 1$ .

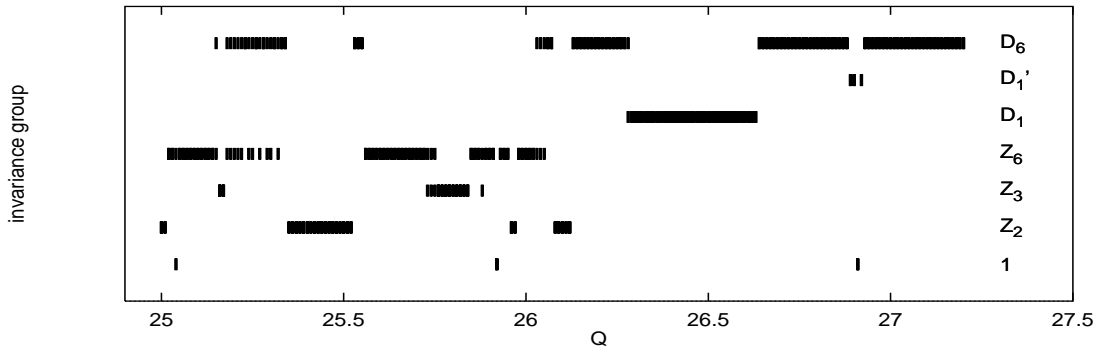


Figure 12: Final symmetry attributions versus  $Q$ . Notice that symmetries  $\mathbf{D}_2$ ,  $\mathbf{D}_3$  and  $\tilde{\mathbf{D}}_3$  never appear.

depends on it considerably.

We do not show plots for  $g = \kappa\zeta^3, \kappa\zeta^4$  and  $\kappa\zeta^5$  since we found that  $r_g = 1$  for these elements if and only if  $r_{\kappa\zeta^2} = 1$  (within statistical errors, of course). Thus for all values of  $Q$  the symmetry group  $\Sigma_Q$  either contains all the elements  $\kappa\zeta^2, \kappa\zeta^3, \kappa\zeta^4$  and  $\kappa\zeta^5$ , or none of them. This implies that none of the attractors had  $\mathbf{D}_2$ ,  $\mathbf{D}_3$ , or  $\tilde{\mathbf{D}}_3$  as its symmetry group, since all these groups (including all their conjugates) contain some elements of the set  $\{\kappa\zeta^2, \kappa\zeta^3, \kappa\zeta^4, \kappa\zeta^5\}$  but not all of them.

For most values of  $Q$  this gave unique symmetry attributions, except for very few points mostly near  $Q \approx 25.2$ . In this range, the orbit switches occasionally between different geometric objects (which are of course not attractors in the strict sense), with vastly different time scales. This had already been noticed in [11]. As an example we show in fig.11 the correlation sum ratio for  $g = \kappa$ ,  $\epsilon = 0.36$  and  $Q = 25.22$  as a function of time. For this figure, a very long trajectory ( $t = 5 \times 10^5$  and  $5 \times 10^5$  points as well) was partitioned into 100 pieces, and correlation sums were computed for each piece separately. We see how  $r_\kappa$  switches between 0 and 1,

with a typical time scale of  $10^4$ .

If this time scale is comparable to the time span covered by the set  $X$ , the latter looks as if obtained from a superposition of two or more measures. The same is obtained if part of the time series comes from a very long lived repeller. It is not easy to distinguish between these two possibilities using correlation sums only. But the presence of either of them is easily recognized in figs.5-10, since  $r_g(\epsilon)$  is roughly independent of  $\epsilon$  except for very small and very large values of the latter.

Our final results are shown in fig.12 where we have indicated the invariance group for every  $Q$ . Multiple entries result from coexisting attractors and/or from the above ambiguity.

When comparing these results with those of [11], we observe several differences: (a) We see much more structure simply because we use a finer sampling in  $Q$  ( $\Delta Q = 0.01$  instead of 0.05 resp. 0.1). For that reason some of the very narrow windows as those at  $Q = 25.92$  and at  $Q = 25.96 - 25.97$  with  $\Sigma = \mathbf{1}$  and  $\mathbf{Z}_2$  were simply missed in [11].

(b) The window at  $Q = 26.89 - 26.92$  with symmetries  $\mathbf{1}$  and  $\tilde{\mathbf{D}}_1$  was presumably missed in [11] since it becomes visible only after a very long transient has died out. A long transient (and not intermittency as suggested in [11]) is also the reason for the transition from  $\mathbf{D}_2$  to  $\mathbf{D}_6$  at  $Q = 26.15$  found in [11].

(c) The same trivial reason might also explain why the large region with  $\mathbf{Z}_3$  symmetry at  $25.74 \leq Q \leq 25.84$  has been missed in [11]. But there is also the more interesting possibility that it was missed since the attractor there is nearly (but not quite!) symmetric under the “rotation”  $g = \zeta$ . As we can see from fig.5, we have to go to rather small distances to see unambiguously that  $r_\zeta(\epsilon) \neq 1$ , and this might easily be overlooked when using detectives.

(d) For most points in the interval  $25.18 \leq Q \leq 25.32$  we find the intermittent behavior illustrated in fig.11 which suggests that the actual symmetry is the full  $\mathbf{D}_6$ . In contrast, the authors of [11] quote  $\mathbf{Z}_6$  for  $Q = 25.2$  and  $Q = 25.3$ , which is the symmetry observed during the (short) times when the curve in fig.11 is below 1 (see also the discussion in [11] concerning  $Q = 25.55$ ).

(e) For  $25.35 \leq Q \leq 25.52$  we observe a large window with very clean  $\mathbf{Z}_2$  symmetry, while [11] quotes  $\mathbf{Z}_6$  also for  $Q = 25.4$ . The reason for this discrepancy is not clear to us. There is a  $\mathbf{Z}_6$ -symmetric transient, but its life time  $t_{trans} \approx 100$  should be too small to have created any confusion.

## 4 Conclusion

We have shown that cross correlation sums are very efficient for studying symmetries of strange attractors. They are numerically more cumbersome than the “detectives” used in [11, 9, 10, 6], but they can be used for smaller data sets and they give much more detailed information. In particular, they allow easily to estimate the amount by which a symmetry is violated.

We tested our method on a model with  $\mathbf{D}_6$  symmetry studied by means of detectives in [11]. We succeeded to obtain unique symmetry attributions even for control parameter values where the authors of [11] failed in spite of much larger data sets. Part of the reason for this is due to rather trivial modifications which are independent of the method used for symmetry detection. These include discarding very long transient and using decimated time series (eventually with irregular time gaps, in order not to be influenced by commensurability effects between the sampling frequency and some periodicity of the attractor). But even taking this into account, it seems that our method makes more complete use of the information contained in a given time series.

Just as the authors of [11], we did not bother with formal statistical error estimates. Nevertheless, and in spite of the small samples used (5000 points), we feel that purely statistical errors were not a serious problem in the present application. Whenever we found an ambiguity, it was due to systematic effects (long transients and/or huge intermittency time scales) which cannot be estimated reliably by any method. At least, our method issues a warning in such a case in form of near-constant cross correlation ratios.

In addition, of course, the estimation of correlation sums allows also to study scaling properties of the attractor. Usually, correlation sums are computed only for that purpose, i.e. in order to estimate attractor dimensions. We have not yet mentioned them here on purpose, to stress that correlation sums contain much more useful information than just dimensions. Nevertheless, we might take the chance here to say that the attractor dimensions indicated by figs. 1-4 are between 2 and 5.

For discussions we thank H.-M. Bröker, H. Frauenkron, F. Krause, T. Schürmann and M. Dellnitz. This work was partly supported by the Deutsche Forschungsgemeinschaft within SFB 237 and Graduiertenkolleg “Feldtheoretische und numerische Methoden in der Statistischen und Elementarteilchenphysik”.

## References

- [1] H. Fujisaka and T. Yamada, Prog. Theor. Phys. **69**, 32 (1983)
- [2] A. Pikovsky, Zeitschr. Physik **B55**, 149 (1984)
- [3] A. Pikovsky and P. Grassberger, J. Phys. **A 24**, 4587 (1991)
- [4] P. Grassberger and A. Pikovsky, in *Renormalization Group '91*, p. 280, D.V. Shirkov *et al.* eds. (World Scientific, Singapore 1992)
- [5] P. Ashwin, Phys. Lett. **A 209**, 338 (1995)
- [6] P. Chossat and M. Golubitsky, Physica **D32**, 423 (1988)
- [7] M.J. Field and M. Golubitsky, *Symmetry in Chaos* (Oxford Univ. Press, Oxford 1992)
- [8] G.P. King and I.N. Stewart, Biol. Cybern. **68**, 287 (1993)
- [9] E. Barany, M. Dellnitz, and M. Golubitsky, Physica **D67**, 66-87 (1993).
- [10] M. Dellnitz, M. Golubitsky and M. Nicol, *Symmetry of Attractors and the Karhunen-Loève Decomposition*, in Appl. Math. Sci. **100**, p.73 (Springer, New York 1994)
- [11] M. Kroon and I.N. Stewart, Intern. Jour. Bif. Chaos **5**, 209 (1995).
- [12] J.-P. Eckmann and D. Ruelle, Rev. Mod. Phys. **57**, 617 (1985)
- [13] H. Kantz, Phys. Rev. **E49**, 5091 (1994).
- [14] J. Theiler, Phys. Rev. **A 34**, 2427 (1986)
- [15] J.J. Collins and I.N. Stewart, Biol. Cybern. **68**, 287 (1993).
- [16] W.A. Brock, D.A. Hsieh and B. LeBaron, *Nonlinear Dynamics, Chaos and Instability: Statistical Theory and Economic Evidence* (MIT press, Cambridge, 1991)
- [17] K. Wu, R. Savit and W. Brock, Physica **D69**, 172 (1993)